Received: 27 May 2021 | Accepted: 24 September 2021

DOI: 10.1002/bab.2271

ORIGINAL ARTICLE

WILEY

An electrochemical aptasensor for detection of prostate-specific antigen using reduced graphene gold nanocomposite and Cu/carbon quantum dots

Golnaz Mehdipour[1] | **Javad Shabani Shayeh**[1] | **Meysam Omidi**[1] | **Mehrab Pour Madadi**[1] | **Fatemeh Yazdian**[2] | **Lobat Tayebi**[3]

[1] Protein Research Center, Shahid Beheshti University, Tehran, Iran

[2] Department of Life Science Engineering, Faculty of New Science and Technologies, University of Tehran, Tehran, Iran

[3] Marquette University School of Dentistry, Milwaukee, Wisconsin, USA

Correspondence
Javad Shabani Shayeh, Protein Research Center, Shahid Beheshti University, P. O. 1983963113, Tehran, Iran.
Email: j_shabani@sbu.ac.ir

Abstract

We report a label-free electrochemical aptamer-based biosensor for the detection of human prostate-specific antigen (PSA). The thiolate DNA aptamer against PSA was conjugated to the reduced graphene oxide/Au (RGO-Au) nanocomposite through the self-assembly of Au-S groups. Owing to the large volume to surface ratio, the RGO-Au nanocomposite provides a large surface for aptamer loading. The RGO-Au/aptamer was combined with a Nafion polymer and immobilized on a glassy carbon electrode. The interaction of aptamer with PSA was studied by cyclic voltammetry, square wave voltammetry, and electrochemical impedance spectroscopy. The detection of limit for prepared electrode was obtained about 50 pg/mL at the potential of 0.4 V in potassium hexacyanoferrate [$K_4Fe(CN)_6$] medium. To decrease the limit of detection (LOD) and applied potential of the prepared nanoprobe Cu/carbon quantum dots (CuCQD) is introduced as a new redox. The results show that this new electrochemical medium provides better conditions for the detection of PSA. LOD of a nanoprobe in CuCQD media was obtained as 40 pg/mL at the potential of −0.2 V. Under optimal conditions, the aptasensor exhibits a linear response to PSA with a LOD as small as 3 pg/mL. The present aptasensor is highly selective and sensitive and shows satisfactory stability and repeatability.

KEYWORDS

Cu carbon quantum dot, electrochemical aptasensor, prostate-specific antigen, quartz crystal microbalance, reduced graphene oxide/gold nanocomposite

Abbreviations: PSA, prostate-specific antigen; RGO-Au, reduced graphene oxide/Au; CV, cyclic voltammetry; SW, square wave voltammetry; EIS, electrochemical impedance spectroscopy; Cu/CQD, Cu carbon quantum dot; PCa, Prostate cancer; GCE, glassy carbon working electrode; DLS, Dynamic light scattering; ELISA, Enzyme-Linked Immunosorbent Assay; NaOH, sodium hydroxide; SELEX, systematic evolution of ligands by exponential enrichment; QCM, quartz crystal microbalance; NaBH4, Sodium borhydrate; K4[Fe(CN)6], potassium hexacyanoferrate.

1 | INTRODUCTION

Prostate cancer is the second most diagnosed cancer and the second cause of mortality in men worldwide.[1] During the past decades, the early diagnosis and increased public awareness led to improved survival rates and prognosis.[2] Therefore, early detection through digital rectal examination and prostate-specific antigen (PSA) serum test would be beneficial in decreasing the growing mortality rate of this common cancer.[3] It has been proven that cancer biomarkers as a sign of abnormal conditions of the disease are promising tools for cancer early detection.[4] The normal range of PSA is related to the age, for men below fifties, the PSA of more than 2.5 ng/mL is considered abnormal, and for the sixties this magnitude is more than 4.0 ng/mL. Therefore, a sensitive and selective method is required to detect minor changes in the levels of the biomarkers. In recent years, aptamers have attracted considerable attention as promising molecular probes for biomarker detection. Aptamers are single strands of oligonucleotides (DNA or RNA) isolated through an in vitro selection called SELEX (systematic evolution of ligands by exponential enrichment). They are capable of binding to various targets ranging from small molecules to the whole cell with high specificity and affinity.[5,6] Aptamers offer several advantages over established antibodies, including high chemical stability, low immunogenicity, simple cell-free synthesis, and easy modification.[7,8] Different aptamer-based biosensors with various transducers such as optical, electrochemical, and mass-sensitive transducers have been developed.[9] Electrochemical methods are considered promising among the various techniques due to their simplicity of fabrication, high sensitivity, and lower cost.[10] To improve the performance of electrochemical aptasensors, different nanomaterials are used to amplify the electrochemical signals of the aptasensors by increasing their recognition surface.[11] Among these nanomaterials, graphene gold nanocomposites with intrinsic advantages of high surface area, excellent electron conductivity, good mechanical strength, and easy functionalization have attracted much attention.[12] Moreover, quartz crystal microbalance (QCM), as a mass-sensitive biosensor that detects small changes in mass around nanograms, is widely used in aptasensors for protein detection for real-time and label-free detection.[13] Based on the piezoelectric effect, the frequency change is proportional to the mass change on the surface of the crystal[14] In this study, we fabricate an electrochemical biosensor for PSA detection based on self-assembly of specific thiolated aptamer onto reduced graphene oxide/Au nanoparticle (RGO-AuNP) nanocomposite at the electrode surface. The biosensor response was checked using cyclic voltammetry (CV), square wave voltammetry (SWV), and electrochemical impedance spectroscopy (EIS) techniques in both hexacyanoferrate and carbon dot/copper as redox probes. The QCM experiment was also performed as another approach for PSA detection using PSA aptamer to verify electrochemical measurements.

2 | EXPERIMENTAL

2.1 | Materials and apparatus

Analytical grade graphite powder, sodium borhydrate ($NaBH_4$), $HAuCl_4{\cdot}4H_2O$, potassium hexacyanoferrate ($K_4[Fe(CN)_6]$), diammonium hydrogen citrate, and $CuCl_2{\cdot}H_2O$ were all purchased from Sigma-Aldrich (Germany) and were used as received. All solutions were prepared using ultrapure water.

The PSA aptamer with 5′SH modification and HPLC purification was synthesized by Bio Basic Inc. (Canada) with the following sequence:

5′ TTT TTT TTT TAT TAA AGC TCG CCA TCA AAT AGC TGC 3′

The lyophilized aptamer powder was diluted by phosphate buffer saline (pH 7.4) and restored at −20°C.[15]

The electrochemical experiments were fulfilled using a Vertex. one electrochemical analysis system (Ivium Technologies, the Netherlands) driven by Ivium soft software provided by the company. A three-electrode system consisted of a glassy carbon working electrode (GCE), a platinium counter electrode, and an Ag/AgCl reference electrode as counter and reference electrodes, respectively. CV, SWV, and EIS were done in 0.2 mM $K_4[Fe(CN)_6]$ and 5 mM Cu/carbon quantum dots CuCQD) as the redox probes. EIS analysis was performed in 0.2 mM $Fe(CN)_6^{3-/4-}$ at the frequency range of 100 mHz to 10 kHz. QCM experiments were performed using an open QCM instrument (Novaetech, Italy). The AT-cut quartz crystal with a resonance frequency of 10 MHz with gold coating on both sides was purchased from Novaetech (Novaetech, Italy). X-ray diffraction (XRD) measurements were performed using an X-ray diffractometer (STOE, Germany), transmission electron microscopic images (TEM, Philips Tecnai G220, operated at 120 kV), FT-IR spectra (Thermo Incol, USA), and dynamic light scattering (DLS) was done on a (Nano Phox, Germany) instrument. All measurements were performed at room temperature. Enzyme-linked immunosorbent assay (ELISA) was done using a UV-2550 spectrophotometer (Shimadzu, Japan).

3 | METHODS

3.1 | Synthesis of graphene oxide

We used the Hummer method for graphene oxide (GO) preparation. To illustrate, 1 g of graphite was dissolved in 20 mL sulfuric acid (98% purity) in an ice bath on a stirrer. After 30 min, 3 g of potassium permanganate was slowly added to the solution until the color turned sludge green. Then after 30 min, 30 mL of distilled water was added dropwise to the mixture. After 10 min, 100 mL of distilled water was added to the solution. Then 30 min later, 35 mL of hydrogen peroxide was added to the obtained solution dropwise. Finally, after 24 h under constant stirring, the mixture was centrifuged, and the precipitate phase was collected and washed with distilled water and ethanol and dried with a freeze dryer.[16,17]

3.2 | Synthesis of RGO-Au nanocomposite

RGO-Au nanocomposite was synthesized using a hydrothermal method. First, 0.6 g of prepared GO was added in 100 mL ultrapure water and was sonicated for 10 min until a homogeneous solution was obtained. Then 1 g of $NaBH_4$ was slowly added to the above solution and was dried at 80°C in the oven overnight to reduce GO. Then the dried powder was rinsed with deionized water and 96% ethanol and undergo centrifuge (5.5 RPM) for 10 min. Next, 0.35 g of reduced GO was dissolved in 80 mL of distilled water and was sonicated for 10 min. Then, 2 mL of 0.25 M $HAuCl_4$ salt was added dropwise to the RGO solution on the constant stirring for 3 h to become combined entirely with RGO. Finally, the solution was centrifuged. The obtained precipitated phase was collected, washed with distilled water and ethanol, and dried with a freeze dryer.[17]

3.3 | Synthesis of CuCQD

CuCQD was synthesized using a hydrothermal method. First, 2 g of di-ammonium hydrogen citrate was dissolved in 75 mL of ultrapure water. Then 1 g of $CuCl_2{\cdot}2H_2O$ was added to the solution. After that, 0.47 g of sodium hydroxide (NaOH) was added to the solution. After NaOH was completely dissolved, the solution was poured into a Teflon-lined stainless-still autoclave reactor (100 mL). Finally, the reactor was placed in a 150°C oven overnight. After completion of the reaction, a dark brown solution was obtained.

3.4 | Electrode modification with Nafion/RGO-Au/apta

First, the glassy carbon electrode ($\Phi = 2$mm) was polished with 0.3 μm alumina slurry and then rinsed with ultrapure water. Then, 2 μL of thiolated aptamer was mixed with 98 μL of 6 mg/mL RGO-Au solution and was incubated at 4°C for 24 h so that the self-assembly of the Au-S group occurs. Then 0.1% Nafion solution was mixed with aptamer/RGO-Au in the proportion of 1:8 to improve the affinity of the composite to the electrode surface. Next, 8 μL of the naf/RGO-Au/apta was dropped on the surface of the prepared GCE and dried at room temperature. Subsequently, 6 μL of PSA antigen with different concentrations was dropped on the naf/RGO-Au/apta. Then the interaction of aptamer/protein was electrochemically examined after 30 min. After each protein adding step, the electrode was gently rinsed with PBS buffer (pH 7.4). The selectivity of the prepared nanoprobe was investigated for PSA (0.1 ng/mL^{-1}) against BSA (0.7 μL/mL), FBS (5 ng/mL), and glucose (90 mg/dL). All the selectivity tests were performed in hexacyanoferrate solution using SW techniques after 30 min of incubation. The results normalized as response percent and compared with the blank medium.

3.5 | QCM modification

The gold-coated quartz crystals were cleaned using a 1:1 mixture of acetone and ethanol for 30 min and then rinsed thoroughly with ultrapure water. All QCM measurements were performed by a flow rate of 0.01 mL/min using a syringe pump. First, 1 mol/L K_2HPO_4 was added to the system to obtain a stable signal. Then a mixed solution of 10 μL PSA aptamer and 490 μL of 1 mol/L K_2HPO_4 was injected into the QCM chamber for self-assembly of thiol on the gold surface of the crystal. The frequency change was measured by comparing the differences in stable signals before and after adding the aptamer. The functionalized electrode was then incubated at 4°C for 24 h for better immobilization. Then it was exposed to 0 ng/mL of PSA protein (control) until reaching a stable signal. This approach was repeated for all the other protein concentrations, including 2.5, 5, 7.5, and 10 ng/mL.

3.6 | Optical characterization of CuCQD biosensor

In order to investigate the interaction between PSA antigen and PSA aptamer with CuCQD, the ELISA test was

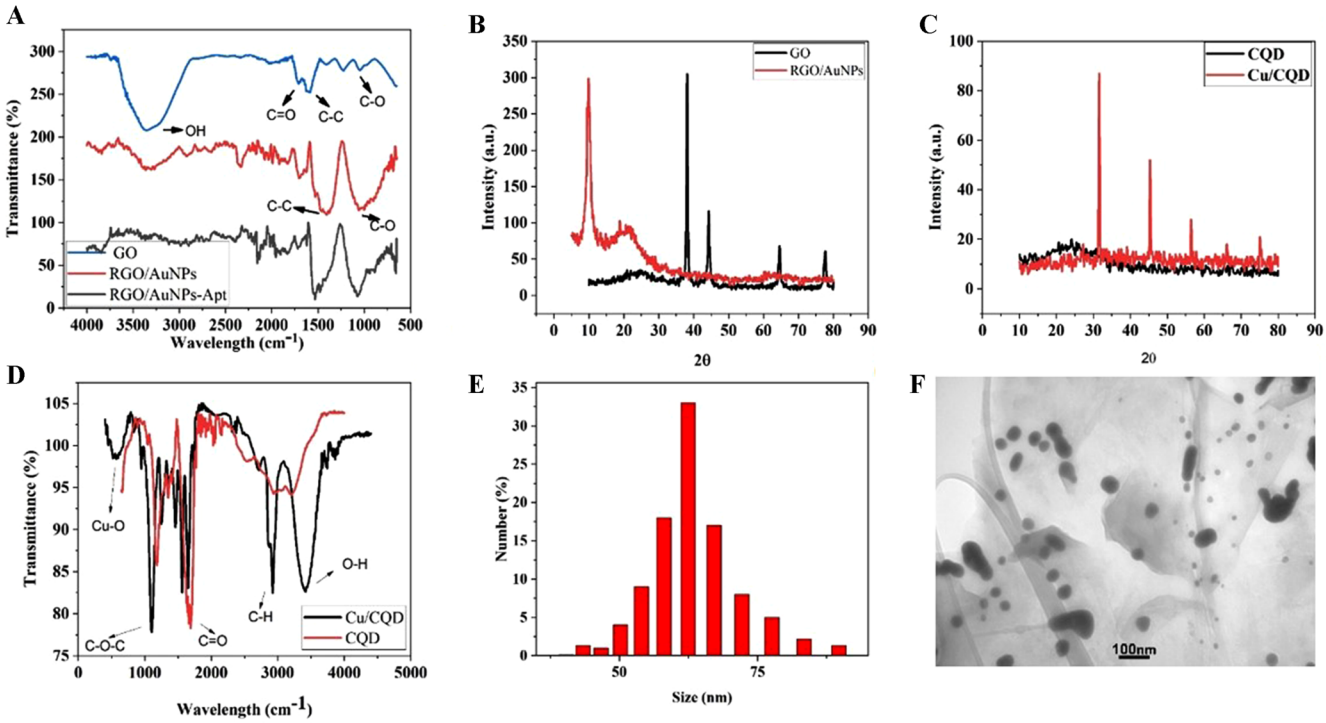

FIGURE 1 (A) The FT-IR spectrum of GO, RGO-Au, and aptamer/ RGO-Au. (B) XRD patterns of GO and RGO-Au, (C) XRD patterns of CQD and CuCQD, (D) FT-IR spectrum of CQD and CuCQD, (E) DLS test and size distribution of the CuCQD, and (f) TEM images of RGO-Au nanocomposite

performed. First, 2 μL of PSA aptamer was added to 2 mg/mL CuCQD solution and then 10 μL of different concentrations of PSA antigen in the range of 2.5, 5, 7.5, and 10 ng/mL were added to the above solution separately. Then each solution was transferred into a clear 96# well plate and read for absorbance at the range of 300–1000 nm. Distilled water was used as a buffer.

4 | RESULTS AND DISCUSSION

Scheme 1 presents the procedure of nanoprobe fabrication. First, synthesized RGO/AuNPs were incubated with aptamer chains and after that dropped on the surface of GCE to prepare the nanoprobe for PSA detection. Figure 1A shows the FT-IR spectra of the graphene oxide, RGO/AuNPs, and RGO/AuNPs-apt. The GO spectrum showed the presence of the O–H group at 3368, C=O at 1733, C=C at 1622, and C–O at 1129 cm.$^{-1}$[18] The noticeable decline in the O–H peak indicates the reduction of GO in the RGO/AuNPs spectrum.[19] By interaction of aptamer chains with RGO/AuNPs, the intensity of O–H peak decreased more due to coverage of RGO/AuNPs surface with aptamer chains. Figure 1B shows the XRD patterns of GO and RGO/AuNPs. The distinct XRD peak at $2\theta = 9.98^{\circ}$ is related to the oxidation of graphite, and the peak at $2\theta =$ 26.01 is related to the (002) plane of graphite that indicates an organized layer structure with an interlayer distance of 0.34 nm.[20] The XRD pattern of RGO/AuNPs showed additional peaks at $2\theta = 38.3^{\circ}$, 44.4°, 64.7°, and 77.7°, which are related to the (111), (200), (220), and (311) plane of Au nanoparticles, respectively.[21] The XRD pattern of CQD and Cu/CQD are presented in Figure 1C. There is a broad peak at $2\theta = 20.66^{\circ}$, which is corresponding to the (002) plane. This indicates the poor crystalline structure of CQD and the presence of more oxygen-containing groups. Moreover, at the XRD spectrum of CuCQD, peaks at $2\theta = 31.58^{\circ}$, 45.35°, 66.14°, and 75.12°, corresponding to (111), (200), (220) and, (311) planes, are for Cu_2O nanoparticles.[22,23] Figure 1D shows the FT-IR spectra of the carbon dot. It revealed the presence of the different functional groups, including OH (3369 cm^{-1}), C–H (2887 cm^{-1}), C=O (1704 cm^{-1}), C–C (1638 cm^{-1}), and C–O–C (1108 cm^{-1}). The CuCQD FT-IR spectrum in Figure 1D shows a significant reduction in C=O moieties and an increase in the amount of O–H groups, which indicates that the groups on the surface of the CQD were reduced to hydroxyl groups partially. Additionally, as it can be observed, the Cu–O band appeared at 556 cm.$^{-1}$[24] The DLS measurement was carried out to confirm the formation of the CuCQD. As Figure 1E shows, the hydrodynamic diameter of the CuCQD is nearly about 60 nm. The hydrodynamic diameter of CQD is significantly increased due to the presence of Cu atoms in the structure of CQD. As shown in Figure 1F, the structure of

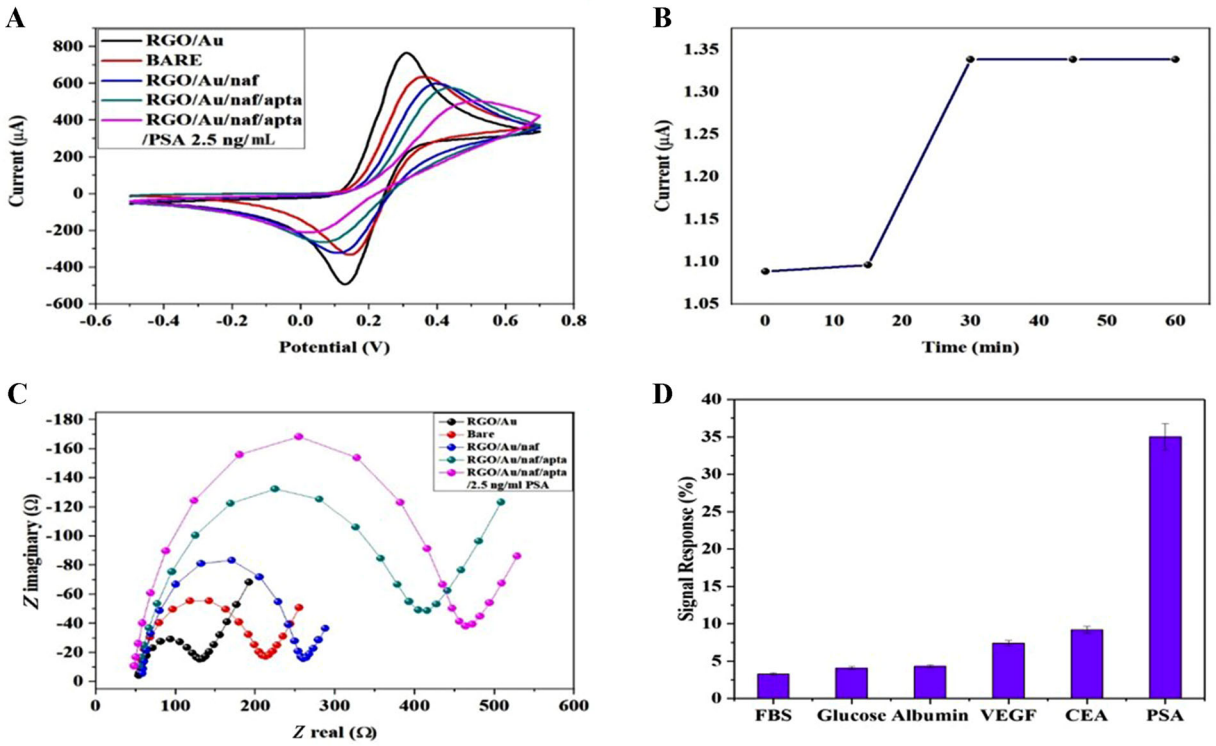

FIGURE 2 (A) CV curves and (B) Nyquist plots of the electrode modification process, (C) effect of the incubation time, and (D) comparison between PSA with FBS, glucose, albumin, CEA, and BSA

synthesized RGO-Au nanocomposite was visualized by TEM images. It can be observed that the gold nanoparticles are uniformly deposited on the surface of RGO with an average size of 50 nm with no visible agglomeration or free particles.

The CV and EIS tests were used to study the fabrication of the aptasensor in each step using [Fe $(CN)_6^{3-/4-}$] redox probe. Figure 2A shows the CVs of different modified electrodes in 0.2 mM [Fe $(CN)_6^{3-/4-}$] at the scan rate of 50 mV/s. As shown, each CV curve has a redox peak due to the electrochemical charge transfer of the $Fe^{+2/+3}$ reaction. The redox peak of RGO/AuNPs is higher than the bare electrode due to the high surface area and good electron conductivity of RGO-Au nanocomposite that facilitates the electron transfer and leads to an increase in peak currents compared to the bare electrode. In the next step, the Nafion polymer was added to the RGO-Au, resulting in a decrease of redox peak currents. This is because the Nafion polymer hinders the diffusion of $Fe(CN)_6^{3-/4-}$ towards the surface of the electrode. In the next level, the PSA antiaptamer was immobilized on the surface of the electrode. This led to a notable decrease in peak current which is due to the electrostatic repulsion of negative-charged phosphates groups on the backbone of the aptamer and the negative ions of the $Fe(CN)_6^{3-/4-}$. When the PSA protein with the concentration of 2.5 ng/mL was bound to the aptamer, the peak current decreased significantly. This is because the formation of the aptamer–protein complex hinders the $Fe(CN)_6^{3-/4-}$ diffusion towards the electrode surface even more. Furthermore, EIS as an effective method was used to examine the fabrication of the nanoprobe by monitoring the changes in charge transfer resistance (R_{ct}). Figure 2B shows the Nyquist plots of the electrode modification process. The semicircle part relates to the electron transfer resistance at high frequencies, and the linear part occurs due to the diffusion process at lower frequencies.[25] When the electrode was modified with RGO-AuNP nanocomposite, it exhibited a smaller R_{ct} than the bare electrode, indicating that the RGO-AuNP has a good electron conductivity. The added Nafion polymer holds back the Fe $(CN)_6^{3-/4-}$ from the electrode surface; therefore, the R_{ct} value increased. Following immobilization of aptamer and PSA, the R_{et} value increased dramatically because of obstruction of the electrode surface and the electrostatic repulsive force of the charged aptamer.

In addition, the nanoprobe's effective incubation time with the PSA antigen was measured. As shown in Figure 2C, with increasing the incubation time from 0 to 60 min, the signal produced by the nanoprobe increased until it reached a plateau at 30 min. That means a saturated binding between nanoprobe and PSA antigen occurs at an optimal incubation time of 30 min. To determine

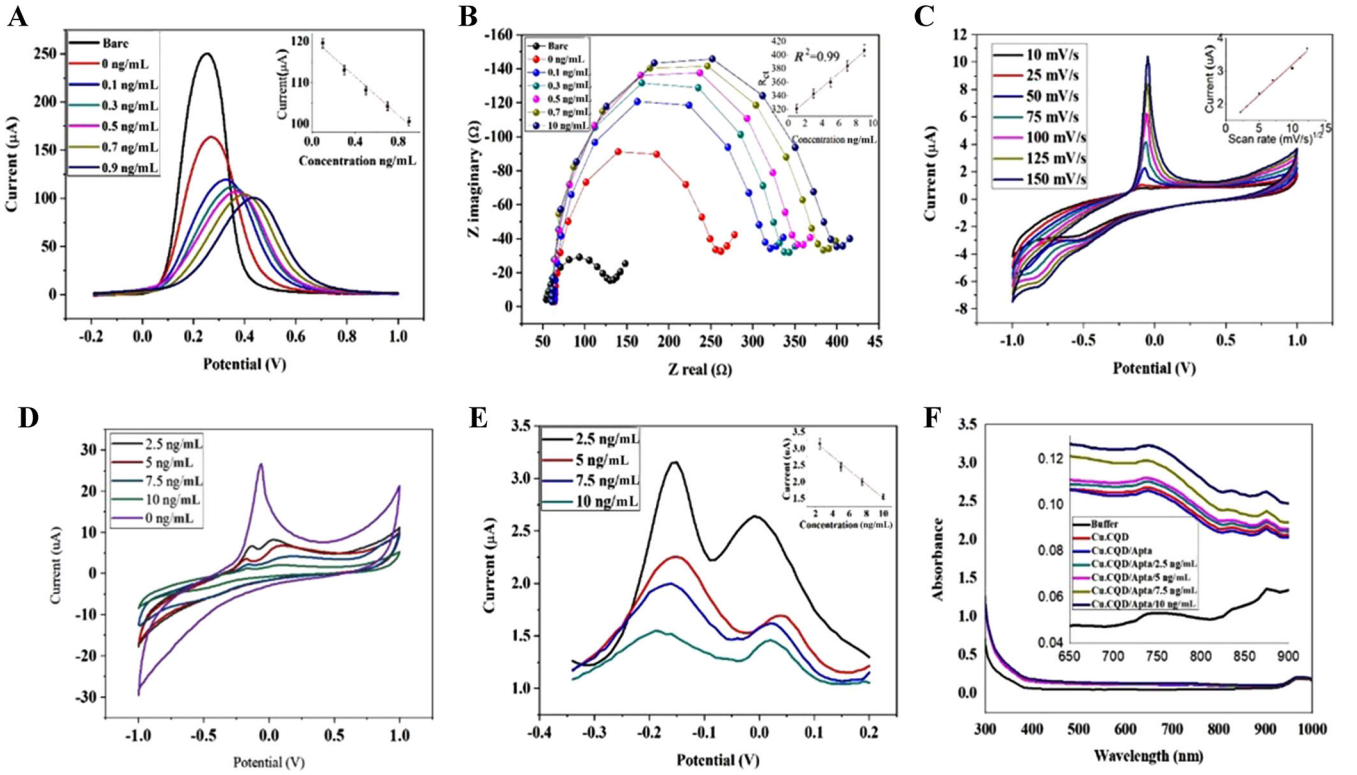

FIGURE 3 (A) SW voltammograms and (B) Nyquist plots of nanoprobe at various concentrations of PSA in hexacyanoferrate solution, (C) CV curves of nanoprobe in 5 mM CuCQD at various scan rates, (D) CVs, and (E) SW voltammograms of nanoprobe at various concentrations of PSA in 5 mM CuCQD, and (F) ultraviolet-visible absorption of the CuCQDs at various concentrations of PSA

the detection specificity of the nanoprobe, its response to some biological molecules such as BSA, glucose, and FBS was investigated. As it can be observed in Figure 2D, no notable changes in nanoprobe response were detected for these biological macromolecules compared to PSA. These observations indicate that the presence of these proteins has a negligible effect on PSA detection and the suggested aptasensor is selective for the PSA antigen. Under the optimized experiment conditions, the analytical performance of the aptasensor for quantitative detecting of PSA antigen with concentrations range of 0.1–0.9 ng/mL is presented in Figure 3. Figure 3A presents the SW voltammograms of the prepared nanoprobe. By increasing the concentration of PSA on the surface of the electrode, the active sites will be blocked; therefore, the current peaks of SWV decreased. The pattern shows that the interaction of PSA and aptamer has a linear behavior that can be used for electrochemical detection.

The Nyquist plots of the modified electrode at various concentrations of PSA were examined to analyze the performance of the aptasensor for PSA detection. As can be seen in Figure 3B, the attachment of PSA macromolecules to aptamer chains increases the surface resistance of the electrode and, therefore, the magnitude of R_{ct} in Nyquist plots increased. The calibration plot between the resistance and the concentration of PSA antigen ranging from 0.1 to 0.9 ng/mL shows an excellent linear relationship (Figure 3B inset). One of the significant results that can be derived from calibration curves is the LOD, which is three times signal to noise ratio. The LOD of the aptasensor was calculated from the following equation:

$$\mathrm{LOD} = \frac{3\sigma}{m}, \tag{1}$$

where σ is the standard deviation of the blank response and m is the slope of the calibration curve. From this equation, the magnitude of LOD was calculated at about 50 pg/mL.

The linear behavior of the electrode shows that this biosensor can be used for the quantitative detection of PSA. Although hexacyanoferrate produces a high electrochemical signal, its hazardous nature emphasizes the use of other electrochemical solutions. For this purpose, we introduce CuCQD as a new synthetic material to act as an electron transfer medium. Figure 3C presents the CV curves of the nanoprobe in a 5 mM CuCQD medium at various scan rates. As illustrated, each CV curve has a sharp oxidation peak and a broad reduction one related to the electrochemical reaction of functional groups at the surface of CuCQD.[26] As can be seen, with increasing the scan rate,

the magnitude of the current peaks increased. That corresponds to the diffusion control process of CuCQD on the surface of the electrode, where the behavior of the peak currents against the scan rate is linear (Figure 3D inset). The quantitative detection of PSA using the CV in CuCQD medium is presented in Figure 6D, whereas in the absence of PSA the CV curve has a redox peak that at the presence of PSA the sharp oxidation peak divided to two oxidation one. Each CV curve has two sharp oxidation peaks followed by a broad reduction one. The difference between CV curves on the presence of PSA molecules is very distinguishable. After adding PSA, a new oxidation peak appeared in CV curves. This new peak can be attributed to the interaction of aptamer with CuCQDs' surface functional groups. As illustrated, by increasing the concentration of PSA, due to the interaction of PSA and aptamer chains, some active sites of the electrode surface got blocked. As the number of active sites at the electrode surface diminished, the peak current of the electrodes decreased. The SWV was also performed for the quantitative detection of the PSA antigen in the CuCQD electrolyte. Figure 3E shows the SWV curves of the electrochemical aptasensor for the nanoprobe-modified electrode in CuCQD solution. Each SWV curve presents two sharp oxidation peaks attributed to the interaction of aptamer with the CuCQDs functional group. With the increase of the PSA concentration, the peak current of the electrodes decreased gradually. The calibration plot between the peak current and the concentration of PSA antigen ranging from 2.5 to 10 ng/mL with an excellent linear relationship. The LOD of the prepared aptasensor using CuCQD as electrolyte was calculated as 40 pg/mL.

Figure 3F shows the ELISA spectrum of the CuCQD/apta/PSA solution in the wavelength range of 300–1000 nm and the selected range of 650–900 nm (inset). As shown, the absorbance decrease after the aptamer was added. However, it could be clearly observed that in the presence of different concentrations of PSA antigen, the absorbance of the CuCQD/Apta solution increased gradually. This confirms the reaction between the PSA antigen and CUCQD and the appearance of the second peak in the electrochemical CV and SWV of the CuCQD after adding PSA. Distilled water was used as a control buffer.[27] Figure 4A shows the frequency change of QCM electrode modified by aptamer chains at various concentrations of PSA. The aptamer chains bonded to the gold electrode surface through Au-S binding. By increasing the concentration of PSA antigen at the surface of the QCM electrode, the resonance frequency of the gold electrode changed. It occurs because of the interaction between antigen molecules and aptamer chains, which

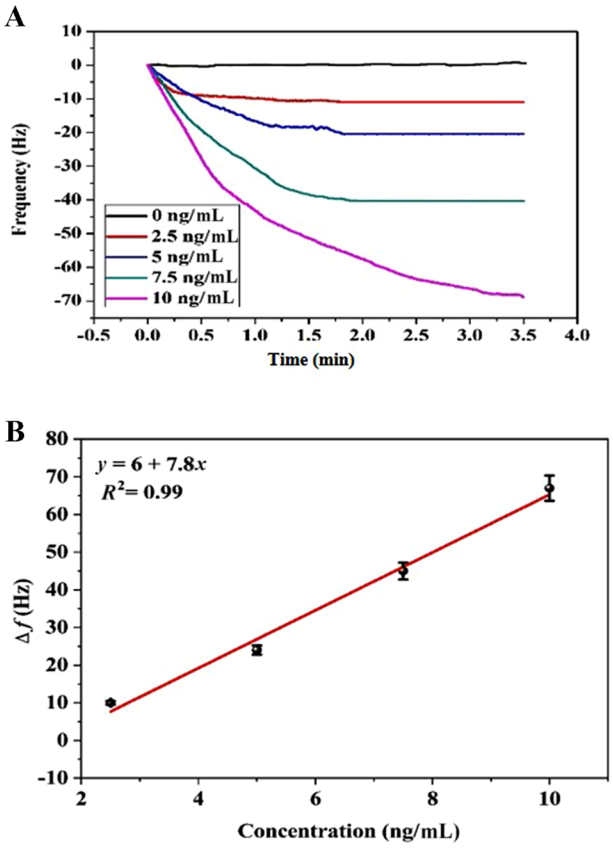

FIGURE 4 (A) The resonance frequency of QCM electrode as a function of time for different concentrations of PSA and (B) calibration plot between the frequency change and the concentration of PSA

causes an increase in weight on the electrode surface. A good linear relationship between the frequency change and concentration of PSA from 2.5 to 10 ng/mL was obtained. The linear response of the QCM electrode to PSA concentrations shows the capability of using the electrode for PSA detection with the LOD of 3 pg/mL (Figure 4B). Stability and reproducibility are two significant factors of a biosensor electrode. To analyze the stability, the electrode was stored in a refrigerator for 3 days, and the results show that the electrode has suitable stability for PSA determination. Furthermore, five electrodes prepared from different batches were tested in the presence of 0.5 ng/mL PSA with a relative standard deviation of 3% that indicates the good reproducibility of the biosensor electrode.

Finally, the prepared biosensor was compared with the other PSA biosensor (Table 1). The results show that the biosensor has suitable performance for the determination of PSA and can be used for clinical applications.

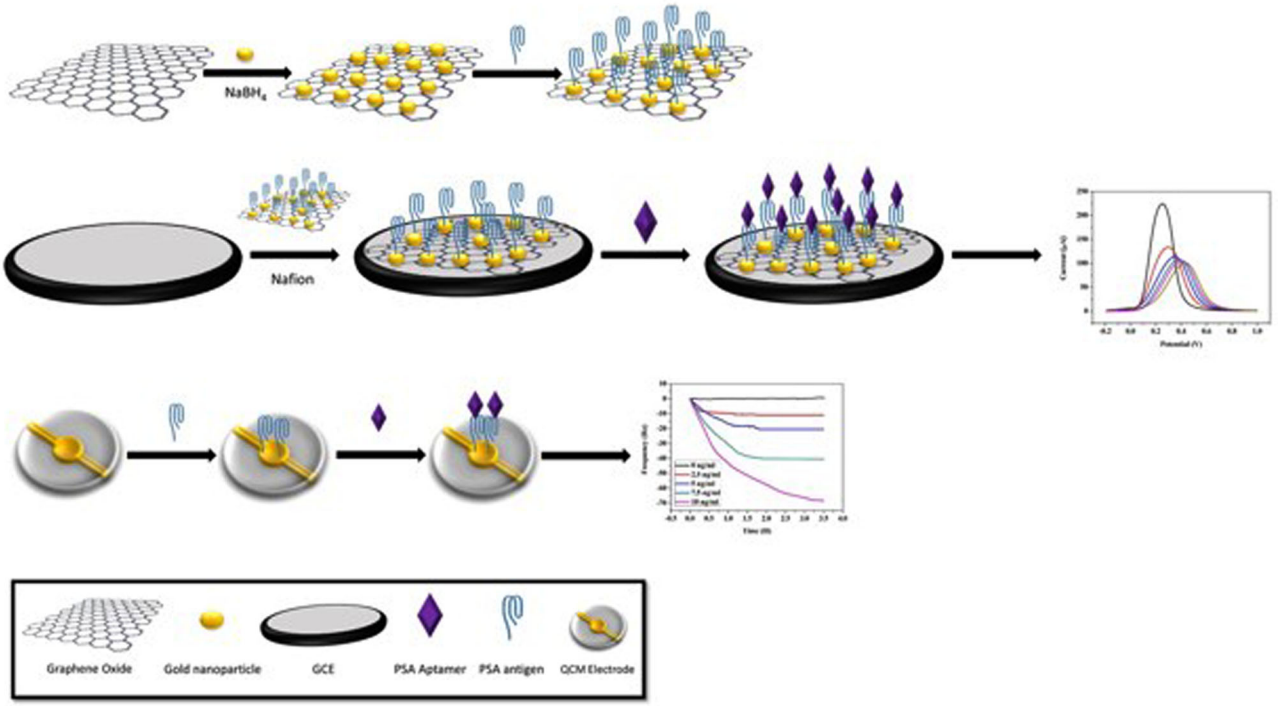

SCHEME 1 Procedure for the fabrication of RGO-Au/apta nanoprobe for the detection of PSA antigen

TABLE 1 Comparison of the prepared nanobiosensor with other PSA biosensor reported

Type of nanobiosensor	Component	Range of detection	Limit of detection	Ref.
Electrochemical	Graphene oxide/ssDNA/PLLA nanoparticles	1–100 ng/mL	1 ng/mL	28]
Electrochemical	Peptide nanotube, gold nanoparticle, and polyaniline composite	1–100 ng/mL	0.68 ng/mL	29
Electrochemical	Graphene oxide–gold nanostructures	0–10 ng/mL	0.2 ng/mL	30
Electrochemical	Gold nanoflowers and DNA tetrahedron structural probes	1–100 ng/mL	0.2 ng/mL	31
Electrochemical	antibody/HRP-labelled Au nanoparticles	1–13 ng/mL	0.2 ng/mL	32
Electrochemical	Reduced graphene gold nanocomposite and Cu/Carbon Quantum Dots	0.1–0.9 ng/mL	50 pg & 40 pg	This study
QCM	gold nanoparticles	0–50.0 μg/L	0.054 μg/L	33
QCM	gold nanoparticles	100–25.0 ng/mL	48 pg mL^{-1}	34
QCM	gold plated electrodes	0.25–2.5×10^3 ng/mL	0.25 ng/mL	35
QCM	gold plated electrodes	4–10 ng/mL	3 pg	This study

5 | CONCLUSION

In this study, a sensitive and selective electrochemical aptasensor for detecting PSA antigen based on RGO/AuNPs-modified electrode was developed. The thiolated aptamer with a high affinity towards the PSA antigen was self-assembled on RGO/AuNPs nanocomposite. The RGO/AuNPs provided a large surface area for aptamer immobilization and improved electron conductivity. The response of the fabricated aptasensor was examined with CV, SWV, and EIS methods in $K_4[Fe(CN)_6]$. It provided a linear range with a detection limit of 50 pg/mL. CuCQD was used as a brand new redox probe with high stability and a well-defined redox signal. The response of the fabricated aptasensor in CuCQD was examined with CV and SWV methods. It showed a linear range with a 40-pg/mL

detection limit at the potential of −0.2 V. The CuCQD optical properties can also be used for optical recognition of the target protein in further studies. To confirm the electrochemical results, the QCM method was also applied for PSA recognition. The PSA aptamer was self-assembled on a QCM gold electrode. By adding the PSA antigen, changes in the frequency were obtained. Furthermore, the presented method can also be applied to detect other cancer biomarkers with related.

ORCID

Javad Shabani Shayeh https://orcid.org/0000-0003-0187-1249

REFERENCES

1. Printz C. Study finds that women with posttraumatic stress disorder have an increased risk of ovarian cancer. Cancer. 2020;126(3):468–9.
2. Mohler JL. The 2010 NCCN clinical practice guidelines in oncology on prostate cancer. Huntington, NY: Harborside Press; 2010.
3. Kawachi MH, et al. Prostate cancer early detection. J Nat Comprehen Cancer Network. 2007;5(7):714–36.
4. Tothill IE. Biosensors for cancer markers diagnosis. Semin Cell Dev Biol. 2009;20(1):55–62.
5. Hori S-i, et al. Current advances in aptamers for cancer diagnosis and therapy. Cancers. 2018;10(1):9.
6. Yu X, et al. Whole-bacterium SELEX of DNA aptamers for rapid detection of E.coli O157:H7 using a QCM sensor. J Biotechnol. 2018;266:39–49.
7. Jolly P, et al. DNA aptamer-based sandwich microfluidic assays for dual quantification and multi-glycan profiling of cancer biomarkers. Biosens Bioelectron. 2016;79:313–9.
8. Kashefi-Kheyrabadi L, et al. Ultrasensitive detection of human liver hepatocellular carcinoma cells using a label-free aptasensor. Anal Chem. 2014;86(10):4956–60.
9. Hashkavayi AB, et al. Ultrasensitive electrochemical aptasensor based on sandwich architecture for selective label-free detection of colorectal cancer (CT26) cells. Biosens Bioelectron. 2017;92:630–7.
10. Zhao J, et al. Apoferritin protein nanoparticles dually labeled with aptamer and horseradish peroxidase as a sensing probe for thrombin detection. Anal Chim Acta. 2013;759:53–60.
11. Choi Y-E, Kwak J-W, Park JW. Nanotechnology for early cancer detection. Sensors. 2010;10(1):428–55.
12. Azimzadeh M, et al. An electrochemical nanobiosensor for plasma miRNA-155, based on graphene oxide and gold nanorod, for early detection of breast cancer. Biosens Bioelectron. 2016;77:99–106.
13. Osypova A, et al. Sensor based on aptamer folding to detect low-molecular weight analytes. Anal Chem. 2015;87(15):7566–74.
14. Marrazza G. Piezoelectric biosensors for organophosphate and carbamate pesticides: a review. Biosensors. 2014;4(3):301–17.
15. Forouzanfar S, et al. Review—A review of electrochemical aptasensors for label-free cancer diagnosis. J Electrochem Soc. 2020;167(6):067511.
16. Hummers W, Offeman R oxide G. Preparation of Graphitic Oxide. J Am Chem Soc. 1958;80:1339. https://pubs.acs.org/doi/pdf/10.1021/ja01539a017
17. Farzadfard A, et al. Modification of reduced graphene/Au-aptamer to develop an electrochemical based aptasensor for measurement of glycated albumin. Talanta. 2020;211:120722.
18. Hashemi M, et al. Self-assembling of graphene oxide on carbon quantum dot loaded liposomes. Mater Sci Eng C. 2019;103:109860.
19. Zhu Z, et al., Preparation and application of thionin-bridged graphene–gold nanoparticle nanohybrids. J Mater Chem B. 2013;1(10):1432–8.
20. Paulchamy B, Arthi G, Lignesh B. A simple approach to stepwise synthesis of graphene oxide nanomaterial. J Nanomed Nanotechnol. 2015;6(1):1.
21. Yadegari A, et al. An electrochemical cytosensor for ultrasensitive detection of cancer cells using modified graphene–gold nanostructures. RSC Adv. 2017;7(4):2365–72.
22. De B, Voit B, Karak N. Carbon dot reduced Cu 2 O nanohybrid/hyperbranched epoxy nanocomposite: mechanical, thermal and photocatalytic activity. RSC Adv. 2014;4(102):58453–9.
23. Swarnkar R, Singh S, Gopal R. Effect of aging on copper nanoparticles synthesized by pulsed laser ablation in water: structural and optical characterizations. Bull Mater Sci. 2011;34(7):1363–9.
24. Zhao L, et al. Chemiluminescence of carbon dots under strong alkaline solutions: a novel insight into carbon dot optical properties. Nanoscale. 2013;5(7):2655–8.
25. Casero E, et al. Differentiation between graphene oxide and reduced graphene by electrochemical impedance spectroscopy (EIS). Electrochem Commun. 2012;20:63–66.
26. Li M, et al. Review of carbon and graphene quantum dots for sensing. ACS Sensors. 2019;4(7):1732–48.
27. Pourmadadi M, et al. A glassy carbon electrode modified with reduced graphene oxide and gold nanoparticles for electrochemical aptasensing of lipopolysaccharides from Escherichia coli bacteria. Microchim Acta. 2019;186(12):787.
28. Pan L-H, et al. An electrochemical biosensor to simultaneously detect VEGF and PSA for early prostate cancer diagnosis based on graphene oxide/ssDNA/PLLA nanoparticles. Biosens Bioelectron. 2017;89:598–605.
29. Vural T, et al. Electrochemical immunoassay for detection of prostate specific antigen based on peptide nanotube-gold nanoparticle-polyaniline immobilized pencil graphite electrode. J Colloid Interface Sci. 2018;510:318–26.
30. Akbari jonous Z, et al. An electrochemical biosensor for prostate cancer biomarker detection using graphene oxide–gold nanostructures. Eng Life Sci. 2019;19(3):206–16.
31. Feng D, et al. DNA tetrahedron-mediated immune-sandwich assay for rapid and sensitive detection of PSA through a microfluidic electrochemical detection system. Microsyst Nanoeng. 2021;7(1):1–10.
32. Uludag Y, et al. An integrated lab-on-a-chip-based electrochemical biosensor for rapid and sensitive detection of cancer biomarkers. Anal Bioanal Chem. 2016;408(27):7775–83.

33. Pohanka M. QCM biosensor for prostate specific antigen assay using antibody–gold particle conjugate. Int J Electrochem Sci. 2021;16:1–9.
34. Kwak J, Lee SS. Highly sensitive piezoelectric immunosensors employing signal amplification with gold nanoparticles. Nanotechnology. 2019;30(44):445502.
35. Su L, et al. Development of novel piezoelectric biosensor using pzt ceramic resonator for detection of cancer markers. In: Prickril B, Rasooly A, editors. Biosensors, and Biodetection. Berlin: Springer; 2017. p. 277–91.

How to cite this article: Mehdipour Golnaz, Shayeh Javad, Shabani Omidi Meysam, Pour Madadi Mehrab, Yazdian Fatemeh, Tayebi Lobat An electrochemical aptasensor for detection of prostate-specific antigen using reduced graphene gold nanocomposite and cu/carbon quantum dots. Biotechnol Appl Biochem. 2022;69:2102–2111. https://doi.org/10.1002/bab.2271